UCLA

Title

Development and preclinical pharmacology of a novel dCK inhibitor, DI-87

Permalink

https://escholarship.org/uc/item/1v4286g2

Authors

Poddar, Soumya
Capparelli, Edmund V
Rosser, Ethan W
et al.

Publication Date

DOI

Peer reviewed

Development and preclinical pharmacology of a novel dCK inhibitor, DI-87

Soumya Poddar, PhD[1], **Edmund V. Capparelli, PharmD**[4], **Ethan W. Rosser, MS**[1,2], **Raymond M. Gipson, PhD**[3], **Liu Wei, PhD**[1], **Thuc Le, PhD**[1], **Michael E. Jung, PhD**[2], **Caius Radu, MD**[1], **Mina Nikanjam, MD PhD**[5]

[1]Department of Molecular and Medical Pharmacology, University of California Los Angeles, Los Angeles, CA

[2]Department of Chemistry and Biochemistry, University of California Los Angeles, Los Angeles, CA

[3]Department of Chemistry and Biochemistry, Santa Clara University, Santa Clara, CA

[4]Division of Host-Microbe Systems, University of California San Diego, San Diego, CA

[5]Division of Hematology-Oncology, University of California San Diego, La Jolla, CA

Abstract

Background—Deoxycytidine kinase (dCK) is an essential enzyme for production of nucleotides via the salvage pathway; DI-87 is a novel dCK inhibitor in preclinical development for use in anticancer therapy. The current study utilizes PET imaging to evaluate PK-PD relationships and to determine optimal dosing of the drug.

Methods—NSG mice bearing CEM tumors had plasma and tumor PK assessed using mass spectrometry following oral administration of DI-87. dCK inhibition was assessed after a single dose of oral DI-87 followed by a [18F]CFA PET probe and PET imaging. Tumor growth inhibition was assessed by orally administering DI-87 with concurrent intraperitoneal thymidine.

Results—DI-87 had an *in vitro* EC$_{50}$ of 10.2 nM with low protein binding. Peak DI-87 concentrations were observed between 1–3 hours and 3–9 hours in plasma and tumor, respectively, with tumor concentrations less than one third of plasma. Full dCK inhibition, as evaluated by PET imaging, was observed as early as 3 hours following 25 mg/kg dosing and was maintained for 12 hours, with full recovery of enzyme activity after 36 hours. When DI-87 was administered as repeated doses in combination with thymidine, full dCK inhibition was maintained at 12 hours (25 mg/kg twice daily dose) and led to maximal tumor growth inhibition.

Conclusions—DI-87 is a promising new compound for use in combination therapy against tumors expressing dCK. Utilizing a [^{18}F]CFA PET probe targeting the pathway of interest allowed for efficient and accurate identification of the optimal dose for growth inhibition.

1. INTRODUCTION

Deoxyribonucleotide triphosphates (dNTPs) are required for DNA replication and repair, and are essential for tumor growth. They are synthesized through parallel and convergent *de novo* and salvage pathways which redundantly produce the same dNTPs using different substrates. The *de novo* pathway produces dNTPs from glucose and amino acids, and is dependent upon ribonucleotide reductase (RNR), which is the rate-limiting enzyme in this pathway [1]. Therapeutics such as 3-aminopyridine-2-carboxaldehyde thiosemicarbazone (3AP) have been developed to block RNR [2] for anticancer therapy. However, tumors develop resistance through upregulation of salvage pathways which produce dNTPs from preformed deoxyribonucleosides present in the extracellular environment. Deoxycytidine kinase (dCK), a salvage pathway enzyme, phosphorylates preformed deoxycytidine to its monophosphate form (dCMP), which is a key precursor for the production of both deoxycytidine triphosphate (dCTP) and thymidine triphosphate (dTTP). DI-39, a reversible high-affinity dCK inhibitor, has previously been shown to inhibit tumor growth when given in combination therapy with thymidine to mice with acute lymphoblastic leukemia (ALL) xenografts [3]. The anti-tumor effects are the result of both the salvage and *de novo* pathways being simultaneously inhibited: the salvage through DI-39-mediated dCK inhibition, and the *de novo* through thymidine-mediated RNR inhibition. (*R*)-DI-87 (DI-87), is a novel small molecule dCK inhibitor developed to be more soluble and metabolically stable than DI-39.

Positron emission tomography (PET) scanning and tracers (PET probes) can assist in assessing drug effects on target pathways. [^{18}F]Clofarabine ([^{18}F]CFA) was previously developed as a PET probe for dCK inhibition [4] and has higher specificity for human dCK when compared to previous generation probes. [^{18}F]CFA is a purine analog which is phosphorylated by dCK to form cell-retained CFA monophosphate, thereby generating a PET-detectable signal. Such tracers can help determine dose-response relationships by directly interrogating the target pathway being altered by the drug. Because of the importance of dCK to the nucleoside salvage pathway of healthy tissues, it is necessary to characterize dose-response relationships for dCK inhibition to determine the optimal inhibition necessary to maximally suppress tumor growth without leading to excess toxicity.

The aim of the current study is to describe the development and characterize the preclinical pharmacology of the prototype dCK inhibitor, DI-87. The study utilizes PET imaging to measure dCK inhibition, and PK-PD modeling to quantify dose-response relationships between tumor drug levels and tumor growth inhibition.

2. MATERIALS AND METHODS

2.1 General chemical methods

Unless otherwise noted, reactions were carried out in oven-dried glassware under an atmosphere of nitrogen using commercially available anhydrous solvents. Solvents used for extractions and chromatography were not anhydrous. 4,6-diamino-2-mercaptopyrimidine was obtained from drying the hydrate over dynamic vacuum at 110 °C for 20 h. All other reagents obtained from commercial suppliers were reagent grade and used without further purification unless specified. Reactions and chromatography fractions were analyzed by thin-layer chromatography (TLC) using Merck precoated silica gel 60 F254 glass plates (250 μm). Visualization was carried out with ultraviolet light, vanillin stain, permanganate stain, or p-anisaldehyde stain. Flash column chromatography was performed using E. Merck silica gel 60 (230–400 mesh) with compressed air. All compounds were characterized by ^{1}H and ^{13}C NMR recorded on ARX500 (500 MHz) or Avance500 (500 MHz) spectrometers, and electrospray mass spectrometry data were collected with a Waters LCT Premier XE time-of-flight instrument controlled by MassLynx 4.1 software. Samples were dissolved in methanol and infused using direct loop injection from a Waters Acquity UPLC into the Multi-Mode Ionization source. The purity of all final compounds was determined to be >95%. Analytical HPLC analysis was performed on a Knauer Smartline HPLC system with a Phenomenex reverse-phase Luna column (5 μm, 4.6×250 mm) with inline Knauer UV (254 nm) detector. Mobile phase: A: 0.1% TFA in H2O, B: 0.1% TFA in MeCN.

2.2 Reagents:Synthesis of 4-methoxy-3-(2-morpholinoethoxy)benzonitrile (Figure 2B, step 1)

To a heterogeneous solution of 4-methoxy-3-hydroxybenzonitrile (2.44 g, 16.4 mmol; Chem-Impex, Wood Dale, IL, USA) and Cs_2CO_3 (10.68 g, 32.8 mmol) in N,N-dimethylformamide (DMF) and acetone (1:1, 60 mL) in N,N-dimethylformamide (DMF) and acetone (1:1, 60 mL) was added 4-(2-chloroethyl)morpholine hydrochloride (2.45 g, 16.4 mmol;Sigma-Aldrich, St. Louis, MO, USA). The reaction solution was stirred under argon at 70 °C for 12 hours. The reaction solution was then filtered and the filtrate diluted with deionized water before extracting three times with ethyl acetate. The combined organic layers were dried over anhydrous $MgSO_4$ and concentrated *in vacuo* before purification by flash chromatography over silica gel (2:3 ethyl acetate/hexanes) to yield the desired product **1** (3.91 g, 91% yield). ^{1}H NMR (500 MHz, CDCl$_3$) δ 7.29 (dd, $J = 8.4, 1.9$ Hz, 1H), 7.13 (d, $J = 1.9$ Hz, 1H), 6.91 (d, $J = 8.4$ Hz, 1H), 4.16 (t, $J = 5.9$ Hz, 2H), 3.91 (s, 3H), 3.73 (t, $J = 4.7$ Hz, 4H), 2.85 (t, $J = 5.9$, 2H), 2.59 (t, $J = 4.6$ Hz, 4H).

Synthesis of 4-methoxy-3-(2-morpholinoethoxy)benzothioamide (Figure 2B, step 2)—To a solution of **1** (1.52 g, 5.79 mmol) in pyridine (12 mL) was added Et$_3$N (1 mL) and ammonium sulfide solution (20 wt% in water, 5.93 mL, 17.4 mmol; Sigma Aldrich,

St. Louis, MO, USA). The reaction solution was stirred for 12 hours at 60 °C, cooled to room temperature and then concentrated *in vacuo*. The resulting residue was taken up in ethyl acetate and washed with deionized water and brine. The organic layer was dried over anhydrous $MgSO_4$, concentrated *in vacuo*, and purified by flash chromatography over silica gel (1:2 to 2:1 ethyl acetate/hexanes) to yield the desired thioamide **2** (1.35 g, 79% yield). ^{1}H NMR (300 MHz, CDCl$_3$) δ 7.75 (br s, 1H), 7.65 (d, *J* = 2.2 Hz, 1H), 7.41 (dd, *J* = 8.5, 2.2 Hz, 1H), 7.36 (br s, 1H) 6.81 (d, *J* = 8.5 Hz, 1H), 4.21 (t, *J* = 5.9 Hz, 2H), 3.88 (s, 3H), 3.72 (t, *J* = 4.7, 4H), 2.85 (t, *J* = 5.9 Hz, 2H), 2.59 (t, *J* = 4.6 Hz, 4H).

Synthesis of 1-(2-(4-methoxy-3-(2-morpholinoethoxy)phenyl)-5-methylthiazol-4-yl)ethan-1-one (Figure 2B, step 3)

To a solution of **2** (276 mg, 0.931 mmol) in ethanol (3 mL) was added 4-bromopentane-2,3-dione (200 mg, 1.12 mmol;Enamine building blocks) and the reaction solution was heated to reflux for 4 hours. The reaction solution was then concentrated *in vacuo*, and the resulting residue was directly purified by trituration with ethyl acetate and hexanes to yield the desired thiazole **3** (190 mg, 54% yield). ^{1}H NMR (500 MHz, CDCl$_3$) δ 7.50 (d, *J* = 2.0 Hz, 1H), 7.47 (dd, *J* = 8.4, 2.1 Hz, 1H), 6.90 (d, *J* = 8.4 Hz, 1H), 4.66 (t, *J* = 4.4 Hz, 2H), 4.30 (s, 2H), 4.02 (s, 2H), 3.88 (s, 3H), 3.72 (s, 2H), 3.55 (t, *J* = 4.3 Hz, 2H), 3.22 (s, 2H), 2.74 (s, 3H), 2.68 (s, 3H).

Synthesis of (S)-1-(2-(4-methoxy-3-(2-morpholinoethoxy)phenyl)-5-methylthiazol-4-yl)ethan-1-ol (Figure 2B, step 4)

To a solution of (*R*)-(+)-2-methyl-CBS-oxazaborolidine (3.0 mL of a 1.0M solution in toluene, 3.0 mmol; Sigma-Aldrich, St. Louis, MO, USA) in THF (13 mL) at −78 °C was added borane–THF complex (4.4 mL of a 1.0M solution in THF, 4.4 mmol), followed by a solution of **3** (125 mg, 0.332 mmol) in THF (7 mL) by syringe pump over 6 hours while stirring at −78 °C. Upon completion of addition by syringe pump, the reaction solution was stirred for another 20 minutes before addition of DI water (10mL) and methanol (5 mL) and warming to room temperature. The aqueous solution was extracted with ethyl acetate, and the resulting organic layer was dried over anhydrous $MgSO_4$ and concentrated *in vacuo*. The resulting residue was purified by flash chromatography over silica gel (1:20 to 1:10 methanol/DCM) to yield the desired alcohol **4** (50 mg, 40% yield). ^{1}H NMR (500 MHz, CDCl$_3$) δ 7.49 (d, *J* = 2.1 Hz, 1H), 7.39 (dd, 8.4, 2.1 Hz, 1H), 6.86 (d, *J* = 8.4 Hz, 1H), 4.93 (q, *J* = 6.4 Hz, 1H), 4.22 (t, *J* = 6.1 Hz, 2H), 3.88 (s, 3H), 3.74 (t, *J* = 4.7 Hz, 4H), 2.86 (t, *J* = 6.1 Hz, 2H), 2.60 (t, *J* = 4.5 Hz, 4H), 2.40 (s, 3H), 1.53 (d, *J* = 6.5 Hz, 3H).

Synthesis of (S)-1-(2-(4-methoxy-3-(2-morpholinoethoxy)phenyl)-5-methylthiazol-4-yl)ethyl 2,2,2-trifluoroacetate (Figure 2B, step 5)

To a solution of **4** (47 mg, 0.124 mmol) in DCM (5 mL) at 0 °C was added trifluoroacetic anhydride (TFAA, 0.07 mL, 0.5 mmol; Sigma Aldrich) slowly. After stirring for 30 minutes at 0 °C the reaction solution was warmed to room temperature prior to quenching with a saturated aqueous solution of sodium bicarbonate. The resulting aqueous solution was extracted with ethyl acetate, the combined organic layers washed with brine, concentrated *in vacuo* and used directly in next step due to instability of the trifluoroacetate **5**. ^{1}H NMR (500 MHz, CDCl$_3$) δ 7.50 (d, 1.9 Hz, 1H), 7.48 (dd, 8.4, 1.8 Hz, 1H), 6.91 (d, *J* = 8.4 Hz, 1H), 6.16 (q,

J = 6.6 Hz, 1H), 4.48 (t, J = 4.4 Hz, 2H), 4.01 (t, J = 4.7 Hz, 4H), 3.88 (s, 3H), 3.51 (t, 4.2 Hz, 2H), 2.52 (s, 3H), 1.81 (d, J = 6.6 Hz, 3H).

Synthesis of (*R*)-2-((1-(2-(4-methoxy-3-(2-morpholinoethoxy)phenyl)-5-methylthiazol-4-yl)ethyl)thio)pyrimidine-4,6-diamine (Figure 2B, step 6, DI-87)
—To a solution of crude **5** (71 mg, 0.15 mmol) and Cs_2CO_3 (195 mg, 0.60 mmol; Sigma Aldrich, St. Louis, MO, USA) from the previous step in DMF was added 4,6-diamino-2-mercaptopyrimidine (43 mg, 0.30 mmol; Sigma Aldrich, St. Louis, MO, USA) and the reaction solution was stirred at 80 °C. After 3 hours, the reaction solution was concentrated *in vacuo* and purified by flash chromatography over silica gel (1:20 to 1:10 methanol/DCM). Additional purification by chiral reverse-phase liquid chromatography (CHIRALPAK IA-3, 4.66 mm x 150 mm, 3 μm) with an n-hexane/EtOH solvent system containing 0.1% TFA (minute/%EtOH: 0/1, 5/1, 35/50, 40/50, 45/0) with detection performed at 254 nm afforded (*R*)-DI-87 in >99% ee (20 mg, 27% yield). ^{1}H NMR (400 MHz, CDCl$_3$) δ 7.54 (d, J = 2.0 Hz, 1H), 7.37 (dd, J = 8.4, 2.0 Hz, 1H), 6.86 (d, J = 8.4, 1H), 5.24 (s, 1H) 5.22 (q, J = 7.0 Hz, 1H), 4.60 (s, 4H), 4.24 (t, J = 5.9 Hz, 2H), 3.88 (s, 3H), 3.76 (t, J = 4.7 Hz, 4H), 2.87 (t, J = 5.9 Hz, 2H), 2.61, (t, J = 4.5 Hz, 4H), 2.50 (s, 3H), 1.80 (d, J = 7.0 Hz, 3H); ^{13}C NMR (125 MHz, CDCl$_3$) δ 170.5, 163.8, 163.3, 153.5, 150.8, 148.4, 127.4, 126.9, 119.9, 111.6, 111.3, 80.7, 67.0, 66.7, 57.6, 56.1, 54.2, 37.7, 22.1, 11.7; HRMS-ESI (m/z) [M + H]$^+$ calcd for $C_{23}H_{31}N_6O_3S_2$, 503.18991, found 503.18727.

2.3 dCK Uptake Assay Performed in Cell Culture

The human cell line CCRF-CEM (CEM) was purchased from American Type Culture Collection (ATCC) with passage number 2–20 used for all experiments. Cells were seeded at a density of 50,000 cells/well in Millipore MultiScreen GV 96 well plates. 0.25 μCi of 3 H-dC (Moravek Biochemicals) were added to the cells simultaneously with varying concentrations of the dCK inhibitor at a final volume of 100 μL/well. After 1 hr at 37 °C, cells were washed four times with ice cold phosphate-buffered saline (PBS) using the Millipore Vacuum Manifold. The amount of incorporated probe was measured by scintillation counting with the PerkinElmer Microbeta.

2.4 Cell proliferation assay

CEM cells were plated at 1×10^3 cells / well in at 50 μl /well in white opaque 384-well plates and treated as described. Following incubation with increasing concentrations (2 nm-10 μM) of gemcitabine ± 1 μM DI-87 for 72 hr, 50 μl of CellTiter-Glo reagent (Diluted 1:5 in dH$_2$O) was added to each well, plates incubated at room temperature for 5 m and luminescence was measured using a BioTek microplate luminescence reader.

2.5 Animals

Animal studies were conducted under the approval of the UCLA Animal Research Committee and were performed in accordance with the guidelines from the Division of Laboratory Animal Medicine at UCLA. All NOD scid gamma (NSG) mice were purchased from the UCLA Radiation Oncology breeding colony.

2.6 Mouse xenograft tumor models and treatments

Mice had three separate evaluation protocols which included pharmacokinetics, dCK activity, and growth inhibition studies. CEM cells were maintained in 10% FBS in RPMI-1640 and were grown at 37°C, 20% O_2, and 5% CO_2. CEM tumor xenografts were developed in 8–12 week-old male or female NSG mice by implanting 2×10^6 CEM cells in 100 μL of a 50/50 (vol/vol) mixture of PBS and matrigel (BD Biosciences) for subcutaneous injections in left shoulders (for imaging, PK, and growth inhibition studies). DI-87 (dCKi, Sundia Pharmaceuticals) was administered by oral gavage to recipient animals. For oral administration of DI-87, the drug was solubilized in the formulation containing PEG-200: Transcutol: Labrasol: Tween-80 mixed in 5:3:1:1 ratio. For imaging studies, the mice were treated with indicated doses of DI-87 after the tumor size reached 250 mm³. For growth inhibition and pharmacokinetic studies, treatments were started after the tumors reached 50 mm³.

2.7 Pharmacokinetic studies of DI-87 in mice

DI-87 plasma and tumor concentrations were assessed at 1, 3, 6, 9 and 24 h following oral administration of 10, 25, or 50 mg/kg of DI-87 to female NSG mice with CEM tumors (N=5 mice per time point). At each time point, a cohort of mice was sacrificed by cervical dislocation; thus, a single plasma and tumor concentration were obtained from each mouse. Blood samples were collected in heparin-EDTA tubes by the retro-orbital technique and spun at 6000 x g for 15 min prior to collecting the plasma supernatants. All plasma samples were frozen at −20°C before sample processing. The stock solutions of DI-87 and DI-82 (internal standard) were prepared by dissolving the appropriate amount of each drug in a known volume of dimethyl sulfoxide (DMSO) to a 10 mM concentration and were stored at −20°C before use. DI-82 (internal standard) was diluted to 200 nM in methanol to make the internal solution. The calibration standards were prepared by spiking working stock solutions of DI-87 in plasma from untreated mice to give 0.01–10 pmol/μL range. Each 20 μL calibration standard sample was mixed with 60 μL of internal solution (methanol with 200 nM internal standard) and vortexed for 30 s. Following centrifugation at 15,000 x g for 10 min, approximately 60 μL of sample was carefully transferred into HPLC injector vials for LC-MS/MS-MRM analysis. Plasma samples were processed the same way as the calibration standard samples. 20 μL samples were injected onto a reverse phase column, (Thermo Scientific Hypersil GOLD column 3.0 μm; 2.1×100 mm) equilibrated in 0.1% water/formic acid, and eluted (200 μL/min) with an increasing concentration of solvent B (acetonitrile/formic acid, 100/0.1, v/v: min/% acetonitrile; 0/0, 5/0, 15/60, 16/100, 19/100, 20/0, and 25/0). The effluent from the column was directed to the Agilent Jet Stream ion source connected to the triple quadrupole mass spectrometer (Agilent 6460) operating in the multiple reaction monitoring (MRM) mode using previously optimized settings. The following drug precursor→fragment ion transitions were used: DI-82 (511→369), DI-87(503→361). The peak areas for each drug (precursor→fragment ion transitions) at predetermined retention times were recorded using the software supplied by the instrument manufacturer (Agilent MassHunter) [5]. The intraday precision based on the coefficient of variation of replicates of the lower limit of quantification (LLOQ) and for quality control (QC) samples are within 15% and the accuracy of LLOQ and QC samples are within 10%.

Tumors were harvested after dissection of mice, weighed, and snap-frozen in liquid nitrogen. PBS containing internal standard (200 μL for 50 mg tumor) was added to the excised tumor and homogenized using a bead beater (BioSpec). The samples were spun down to collect supernatants. The supernatant was further diluted 5 times in PBS (with internal standard), and four parts of methanol (with internal standard) was added and incubated −80°C overnight to precipitate proteins. The samples were spun at maximum speed (16000g) at 4°C, and supernatant collected. Twenty microliter samples were injected onto a reverse phase column equilibrated in water 0.1% formic acid for LC-MS/MS-MRM analysis in positive ion mode as above and compared to calibration standards.

2.8 dCK activity with MicroPET/CT

dCK activity was evaluated following oral administration of 5, 10, or 25 mg/kg of DI-87 to male NSG mice implanted with CEM tumors (N=4 mice per time point). The NSG mice were anesthetized 3 hours prior to imaging and intravenously administered 740 kBq of [18F]CFA PET probe [4]. Thus, each mouse was representative of a single time point and concentration. MicroPET/CT experiments were conducted using G8 microPET/CT system [6,7]. The mice were then positioned in an imaging chamber and data was acquired with the G8 microPET/CT system (Sofie Biosciences). MicroPET data was acquired for 10 min and reconstructed with a statistical maximum *a posteriori* probability algorithm (MAP) into multiple frames. The spatial resolution of PET is ~1.5 mm with 0.4 mm voxel size. CT images are a low-dose 400 μm resolution acquisition with 200 μm voxel size. MicroPET and CT images were co-registered and then quantified by manually drawing three-dimensional regions of interest using Osirix software. The color scale was proportional to tissue concentration, with red being the highest and yellow, green and blue corresponding to the lower values.

2.9 Growth inhibition studies

Male NSG mice implanted with CEM tumors as above were used for growth inhibition studies. Combination therapy of DI-87 with thymidine was used. Treatments of DI-87 and/or thymidine were started after tumor volume reached 50 mm^3. DI-87 was administered at varying doses orally once a day (QD) or twice a day (BID) for 16–18 days while thymidine (2 g/kg) solubilized in saline was administered intraperitoneally BID after start of treatment [3]. Three cohorts of control mice were administered either: (i) intraperitoneal (i.p.) thymidine alone, (ii) Oral DI-87 with i.p saline injections, or (iii) vehicle for oral DI-87 and saline i.p. Tumor growth, as measured by CT, was compared amongst different treatment groups (n=5 mice, 5 tumors/group). Tumor growth was monitored daily by caliper measurements ([(length × width2)/2]) and bi-weekly by CT measurements.

2.10 Pharmacokinetic and pharmacodynamic modeling

Using the computer program NONMEM (version 7.3) with a GNU Fortran G77 Compiler, DI-87 concentration-time data were modeled using first-order conditional estimation (FOCE) method with interaction. Plasma concentrations were assessed with standard PK models which included a depot compartment representing the gut. Tumor concentrations were evaluated with the addition of a separate tumor compartment once plasma

concentrations had been characterized (ADVAN6, TRANS1 subroutine). An exponential-normal distribution error model was used for inter-subject variability.

A combined pharmacokinetic-pharmacodynamic (PK-PD) model was developed using the final DI-87 plasma-tumor PK parameter estimates (Figure 1). The effect compartment (dCK inhibition or growth inhibition) was linked to the tumor concentrations. Linear (slope), Emax, and sigmoid Emax models were tested to determine which were the best fits to the data (see equations below) [8]. The final model was used to simulate dCK inhibition and growth inhibition from a representative mouse for each of the tested DI-87 concentrations.

PD models:

$$A. \; Linear \; (slope): Slope * Conc.$$

$$B. \; E_{max}: E_{max} * \frac{Conc.}{EC_{50} + Conc.}$$

$$C. \; Sigmoid \; E_{max}: E_{max} * \frac{Conc^{Exp}}{EC_{50}^{Exp} + Conc^{Exp}}$$

3. RESULTS

3.1 Development of a highly potent, orally bioavailable dCK inhibitor, DI-87

While our group had previously developed the dCK inhibitors DI-39 and DI-82, each had drawbacks, including poor solubility and sub-optimal PK. In an effort to improve upon previous generation inhibitors, DI-87 (Figure 2A) was synthesized, with the morpholine moiety specifically incorporated to increase solubility. DI-87 was synthesized as follows: an S_N2 reaction between 4-methoxy-3-hydroxybenzonitrile and 4-(2-chloroethyl) morpholine furnished **1** (Figure 2B). Heating with an aqueous solution of ammonium sulfide gave thioamide **2**, which was subjected to Hantzsch thioazole formation conditions to yield thiazole **3**. Asymmetric Corey-Bakshi-Shibata (CBS) reduction of the ketone resulted in the *S*-alcohol **4**, which was converted into the trifluoroacetate **5** and displaced *via* S_N2 reaction by 4,6-diamino-2mercaptopyrimidine to furnish (*R*)-DI-87 (**6**). The IC_{50} values for each enantiomer of DI-87 were determined using a dC uptake assay in CEM cells. (*S*)-DI-87 exhibited a much higher IC_{50} value (468±2.1 nM) relative to (*R*)-DI-87 (3.15±1.2 nM) (Figure 2C). (*R*)-DI-87 treatment rescued CEM cells from the anti-proliferative effects of gemcitabine, a dCK-dependent nucleoside analog prodrug, with an EC_{50} of 10.2 nM (Figure 2D). Additionally, we observed that protein binding of (*R*)-DI-87 (DI-87) is comparatively lower than its predecessor, (*R*)-DI-82 (DI-82), as measured by IC_{50} of the respective dCK inhibitor in presence of bovine serum albumin (BSA) (Figure 2E).

3.2 Pharmacokinetics of DI-87

DI-87 concentrations in plasma and tumor were determined for 3 dose levels: 10, 25, and 50 mg/kg (Figure 3). Plasma and tumor concentrations were obtained at a single time point from each mouse. Plasma DI-87 concentrations peaked between 1 and 3 hours (Figure 3A). Tumor concentrations were lower than plasma and had a later, more sustained peak at 3–9

hours (Figure 3B). Plasma and tumor PK was also evaluated in male mice following a 10 mg/kg dose, with essentially identical results to those seen in female mice (data not shown).

A population PK model was initially developed for plasma concentrations, with a one-compartment structural model fitting the data well. An additional compartment was added to model tumor concentrations. The parameter estimates for the combined tumor and plasma population PK model are shown in Table 1. KA was fixed to the parameter estimate obtained from the plasma PK model. The typical clearance value was 0.46 L/hr/kg and the plasma volume of distribution was 2.78 L/kg. Actual tumor volumes were used in the model. Plasma concentrations were more than 3.5-fold higher than tumor concentrations.

3.3 dCK inhibition studies

DI-87 was administered to mice at three separate doses (5, 10, and 25 mg/kg) to establish a dose response curve. The [18F]CFA PET probe was administered 3 hours prior to imaging. Representative mice at each time point and concentration are shown in Figure 4A, and data from all mice is represented graphically in Figure 4B. The 25 mg/kg dose exhibited full dCK inhibition for 27 hrs, and enzyme activity fully recovered by 36 hrs. The 10 mg/kg dose resulted in full inhibition with recovery initiating at the 12 hr time point. The 5 mg/kg dose resulted in minimal dCK inhibition with rapid recovery.

The quantitative data generated from PET signal intensity was used in a combined population PK-PD model. PK parameters from the final combined plasma-tumor model were fixed and PD parameters were estimated in NONMEM. A sigmoid E_{max} indirect response PD model [9] was found to fit the dCK inhibition data the best:

$$\frac{dA}{dT} = k_{in} * \left(1 - Sigmoid\ E_{max}\right) - k_{out} * A$$

Final parameter estimates from the model are shown in Table 1. E_{max} was 1.20 and EC_{50} was 0.31 μg/mL. The Hill coefficient was 58.6 which was consistent with the full dCK inhibition seen at the 6 hr time point for the 25 and 10 mg/kg doses, and demonstrating that dCK inhibition is essentially a step function at higher concentrations with the transition from no inhibition to full inhibition being achieved over a relatively narrow range of concentrations. Figure 4C is a simulation of the final model to demonstrate PET signal intensity and the dose response curve for dCK inhibition seen with the 5, 10, and 25 mg/kg doses.

3.4 Growth inhibition studies

Based on the results from the dCK inhibition experiments, we predicted close to full dCK inhibition following 25 mg/kg DI-87 dosing. Growth inhibition studies were performed using 25 mg/kg daily of DI-87 in combination with a fixed dose of i.p. thymidine, since DI-87 alone exhibits minimal growth inhibition. Oral DI-87 at 10 mg/kg was given in combination with i.p. thymidine to demonstrate a dose-response relationship with reduced dCK inhibition. Control mice received either intraperitoneal saline injections alone, oral DI-87 with i.p saline injections, or thymidine alone. These results were validated in a repeat study where we explored the effect of full dCK inhibition throughout the dosing interval,

with 25 mg/kg BID of DI-87 administered in combination with a fixed dose of thymidine as the highest dose.. Tumor size was measured every 3 days after the initiation of drug administration. Mice administered thymidine alone or DI-87 alone had tumor growth curves similar to the control (data not shown). Increasing DI-87 doses resulted in reduced tumor growth, consistent with the dCK inhibition seen in the PET scans. The changes in tumor size with time are shown in Figure 5A.

The tumor sizes from the two studies were used in a combined PK-PD model. PK parameters from the final combined plasma-tumor model were fixed and PD parameters were estimated in NONMEM. A superexponential function was found to describe the growth of the control data the best: $Growth(t) = e^{k1 * t^{k2}}$. An E_{max} indirect response PD model [9] was found fit the growth inhibition data the best:

$$\frac{dA}{dT} = k_{in} - k_{out} * \left(1 + E_{max}\right) - \left(56 * k_1 * k_2 * \left(TIME^{k2-1}\right)\right) * A$$

Final parameter estimates from the model are shown in Table 1. E_{max} was 1.06 and EC_{50} was 3.63 μg/mL. The final model was used for simulations of two concentrations (10 mg/kg daily, and 25 mg/kg BID). Figure 5B demonstrates that the final model fit the experimental data well. Thus, maximal dCK inhibition over the 24 hr dosing period results in greater growth inhibition, consistent with the 25 mg/kg BID dose.

4. DISCUSSION

dCK is an intriguing target in anti-cancer therapy as it is a rate limiting enzyme within the salvage pathway of dNTP biosynthesis, and multiple cell lines and tumor samples in the Cancer Cell Line Encyclopedia and The Cancer Genome Atlas, respectively, express this enzyme at higher levels when compared to normal tissue [10]. Among the cancers listed in these resources, leukemias and lymphomas are most prominently featured. While targeting the salvage pathway of dNTP biosynthesis through dCK inhibition is a relatively new approach, the key enzyme of the parallel *de novo* pathway, ribonucleotide reductase (RNR), has been an important target in anticancer therapy for decades. The RNR inhibitor hydroxyurea (HU) has been used clinically for cancer treatment and is in clinical trials for novel applications. 3-AP is also in clinical trials as an anti-cancer agent [11,12]. Although these compounds are able to inhibit RNR, they each possess dose-limiting toxicity and limited efficacy [13,14]. A major resistance mechanism to RNR inhibition therapy is presence of an active dCK-mediated salvage pathway, which may explain the failure of RNR inhibitors such as 3-AP in clinical trials. In an effort to circumvent this resistance mechanism, we developed inhibitors of dCK to be used in combination with RNR inhibition. We previously reported the development of DI-39 [3] and DI-82 [15], which were potent inhibitors of dCK but possessed poor solubility and sub-optimal drug-like properties. To address these shortcomings, we developed DI-87, a potent, specific, soluble, and bioavailable dCK inhibitor which has recently gained FDA Investigational New Drug (IND) approval and will be evaluated in clinical trials shortly.

In line with our previous studies, we determined that the *R*-enantiomer of DI-87 had a significantly higher affinity for dCK when compared with the *S*-enantiomer. The affinity of DI-87 for dCK was further confirmed through a rescue assay in which the growth of CEM cells treated with gemcitabine with and without DI-87 supplementation was monitored. Gemcitabine requires dCK for its cytotoxic effects, and administration of DI-87 fully prevented cytotoxicity following gemcitabine treatment, thereby demonstrating the dCK inhibition of DI-87. Previous generations of reversible dCK inhibitors developed by our group had comparable potency, but did not have optimal biochemical properties. DI-87 improves upon these properties while maintaining low-nM affinity for dCK. In particular, DI-82 was an effective dCK inhibitor but was heavily protein-bound. By comparison, DI-87 retained its potency in the presence of albumin.

The preclinical pharmacology of DI-87 was also evaluated. Plasma concentrations peaked 3 hours after oral administration, while tumor concentrations maintained a peak between hours 3 and 9. Thus, the tumor-to-plasma concentration ratio was dependent upon sampling time. Tumor concentrations were significantly lower than plasma concentrations for all doses tested. The PET probe [^{18}F]CFA was used to quantify dCK activity in tumors, and thus effects of DI-87 upon the target pathway. Given the differential peaks in plasma and tumor concentrations, linking DI-87 tumor concentrations to dCK inhibition provided a more physiologic and mechanistic approach. Our population PK-PD modeling allowed us to describe limited tumor data and link these concentrations to dCK inhibition. Full dCK inhibition occurred at the 10 mg/kg dose and increasing doses led to a longer maintenance of full inhibition. At the highest dose tested (25 mg/kg), full recovery of enzyme activity occurred by 36 hours, with full inhibition being maintained at the 12 hr time point. Our PK-PD model suggested a threshold or rapid switching on-off effect. When evaluated as a single agent, DI-87 was well tolerated at higher doses, but had essentially no ability to inhibit growth (data not shown). When DI-87 was administered as repeated doses in combination with thymidine, full dCK inhibition was maintained at 12 hours (25 mg/kg twice daily dose) and led to maximal tumor growth inhibition. Lower doses led to diminished dCK inhibition with predictable decreases in growth inhibition. Thus, DI-87 appears to have potential as a cancer therapeutic when used in combination with thymidine.

The PET probe used in the current study is a tool to help provide mechanistically-driven rational dosing of DI-87 and similar compounds prior to clinical trials. The use of non-invasive PET probes and scans can greatly aid in drug development. Imaging studies in early phase development can confirm that molecules reach the target tissue and do not accumulate in target sites, can determine dose-target occupancy, and can be used to help critically evaluate similar drug candidates based on responses [16]. Our group developed [^{18}F]FAC (1-(2'-deoxy-2'-[^{18}F]fluoro-β-D-arabinofuranosyl)cytosine) as the first dCK-specific PET probe [6]. This compound has been used in preclinical drug development of small molecule dCK inhibitors [17]. We subsequently developed a more specific probe, [^{18}F]CFA, which was used in the current study to evaluate dCK activity in tumors when treated with a small molecule dCK inhibitor. This probe is also being studied in a clinical trial at our institution to evaluate changes in dCK activity following cancer immunotherapy [18]. PET probes in preclinical and clinical studies can additionally aid in understanding how drug distribution in target tissues and response of the target pathway is modified in the presence of multiple

drugs, as compared to single agent therapy. They can also help evaluate the degree of synergy, appropriate timing of therapies, and dosing amount.

Our growth inhibition studies utilized a fixed dose of thymidine with varying doses of DI-87, and dual inhibition of salvage and *de novo* pathways led to effective tumor growth inhibition when full dCK inhibition was achieved throughout the dosing interval. PET imaging provided valuable information, namely the quantification of dCK inhibition, which enabled a more efficient methodology for dose optimization as it allowed us to determine optimal dosing and schedules without testing a multitude of doses in growth inhibition studies. The DI-87 plasma half-life of 4 hours suggests the need for more frequent dosing to maintain dCK and growth inhibition, however our mechanistic approach which included evaluation of tumor PK and PET imaging allowed us to determine that the 25 mg/kg dose twice daily would be appropriate to maintain dCK inhibition.

The current study was limited in that each time point represented a separate mouse, since the half-life of the probe did not allow for multiple images within the same mouse. The probe required time for optimal diffusion in the tumor, thus we were unable to quantify dCK inhibition at very early time points. PK in the tumor was evaluated in separate mice rather than using a probe to follow drug levels over time. However, similar results were obtained between replicate experiments and results between mice were similar at each time point; thus, this unlikely represents a major limitation. Given small samples sizes in the PK studies and differing tumor studies between experiments, it was difficult to determine if the PK was linear, however the plasma and tumor PK models fit the data well without evidence of non-linear PK. While a fixed dose of i.p. thymidine was used for growth inhibition in the current study, either an IV or oral RNR inhibitor will be necessary for combination therapy in further clinical development.

In summary, the current study describes the preclinical development and pharmacology of a novel dCK inhibitor, DI-87. It provides additional evidence for the value of PET probes in assisting with preclinical drug development. By using a probe specific for dCK activity, we were able to accurately and efficiently predict appropriate dosing for growth inhibition studies by determining a DI-87 dose that resulted in maximal dCK inhibition throughout the dosing interval. We have additionally developed PK-PD models for both dCK inhibition and growth inhibition which can be used to optimize dosing schedules for preclinical studies. Taken together, DI-87 is a promising new compound for combination therapy in tumors expressing dCK.

Acknowledgements/Funding

REFERENCES

1. Reichard P: Interactions between deoxyribonucleotide and DNA synthesis. Annu Rev Biochem 57:349–74, 1988 [PubMed: 3052277]

2. Chao J, Synold TW, Morgan RJ Jr., Kunos C, Longmate J, Lenz HJ, et al.: A phase I and pharmacokinetic study of oral 3-aminopyridine-2-carboxaldehyde thiosemicarbazone (3-AP, NSC #663249) in the treatment of advanced-stage solid cancers: a California Cancer Consortium Study. Cancer Chemother Pharmacol 69:835–43, 2012 [PubMed: 22105720]

3. Nathanson DA, Armijo AL, Tom M, Li Z, Dimitrova E, Austin WR, et al.: Co-targeting of convergent nucleotide biosynthetic pathways for leukemia eradication. J Exp Med 211:473–86, 2014 [PubMed: 24567448]

4. Kim W, Le TM, Wei L, Poddar S, Bazzy J, Wang X, et al.: [18F]CFA as a clinically translatable probe for PET imaging of deoxycytidine kinase activity. Proc Natl Acad Sci U S A 113:4027–32, 2016 [PubMed: 27035974]

5. Le TM, Poddar S, Capri JR, Abt ER, Kim W, Wei L, et al.: ATR inhibition facilitates targeting of leukemia dependence on convergent nucleotide biosynthetic pathways. Nat Commun 8:241, 2017 [PubMed: 28808226]

6. Radu CG, Shu CJ, Nair-Gill E, Shelly SM, Barrio JR, Satyamurthy N, et al.: Molecular imaging of lymphoid organs and immune activation by positron emission tomography with a new [18F]-labeled 2'-deoxycytidine analog. Nat Med 14:783–8, 2008 [PubMed: 18542051]

7. Shu CJ, Campbell DO, Lee JT, Tran AQ, Wengrod JC, Witte ON, et al.: Novel PET probes specific for deoxycytidine kinase. J Nucl Med 51:1092–8, 2010 [PubMed: 20554721]

8. Upton RN, Mould DR: Basic concepts in population modeling, simulation, and model-based drug development: part 3-introduction to pharmacodynamic modeling methods. CPT Pharmacometrics Syst Pharmacol 3:e88, 2014

9. Gobburu JV, Jusko WJ: Role of dosage regimen in controlling indirect pharmacodynamic responses. Adv Drug Deliv Rev 46:45–57, 2001 [PubMed: 11259832]

10. Cerami E, Gao J, Dogrusoz U, Gross BE, Sumer SO, Aksoy BA, et al.: The cBio cancer genomics portal: an open platform for exploring multidimensional cancer genomics data. Cancer Discov 2:401–4, 2012 [PubMed: 22588877]

11. Madaan K, Kaushik D, Verma T: Hydroxyurea: a key player in cancer chemotherapy. Expert Rev Anticancer Ther 12:19–29, 2012 [PubMed: 22149429]

12. Kunos CA, Chu E, Beumer JH, Sznol M, Ivy SP: Phase I trial of daily triapine in combination with cisplatin chemotherapy for advanced-stage malignancies. Cancer Chemother Pharmacol 79:201–207, 2017 [PubMed: 27878356]

13. Murren J, Modiano M, Clairmont C, Lambert P, Savaraj N, Doyle T, et al.: Phase I and pharmacokinetic study of triapine, a potent ribonucleotide reductase inhibitor, administered daily for five days in patients with advanced solid tumors. Clin Cancer Res 9:4092–100, 2003 [PubMed: 14519631]

14. Pelivan K, Frensemeier L, Karst U, Koellensperger G, Bielec B, Hager S, et al.: Understanding the metabolism of the anticancer drug Triapine: electrochemical oxidation, microsomal incubation and in vivo analysis using LC-HRMS. Analyst 142:3165–3176, 2017 [PubMed: 28745337]

15. Nomme J, Li Z, Gipson RM, Wang J, Armijo AL, Le T, et al.: Structure-guided development of deoxycytidine kinase inhibitors with nanomolar affinity and improved metabolic stability. J Med Chem 57:9480–94, 2014 [PubMed: 25341194]

16. Matthews PM, Rabiner EA, Passchier J, Gunn RN: Positron emission tomography molecular imaging for drug development. Br J Clin Pharmacol 73:175–86, 2012 [PubMed: 21838787]

17. Murphy JM, Armijo AL, Nomme J, Lee CH, Smith QA, Li Z, et al.: Development of new deoxycytidine kinase inhibitors and noninvasive in vivo evaluation using positron emission tomography. J Med Chem 56:6696–708, 2013 [PubMed: 23947754]

18. 18F-Clofarabine PET/CT in Imaging Cancer Patients Before and After Interventions. https://clinicaltrials.gov/ct2/show/NCT02888301. Accessed October 8, 2018.
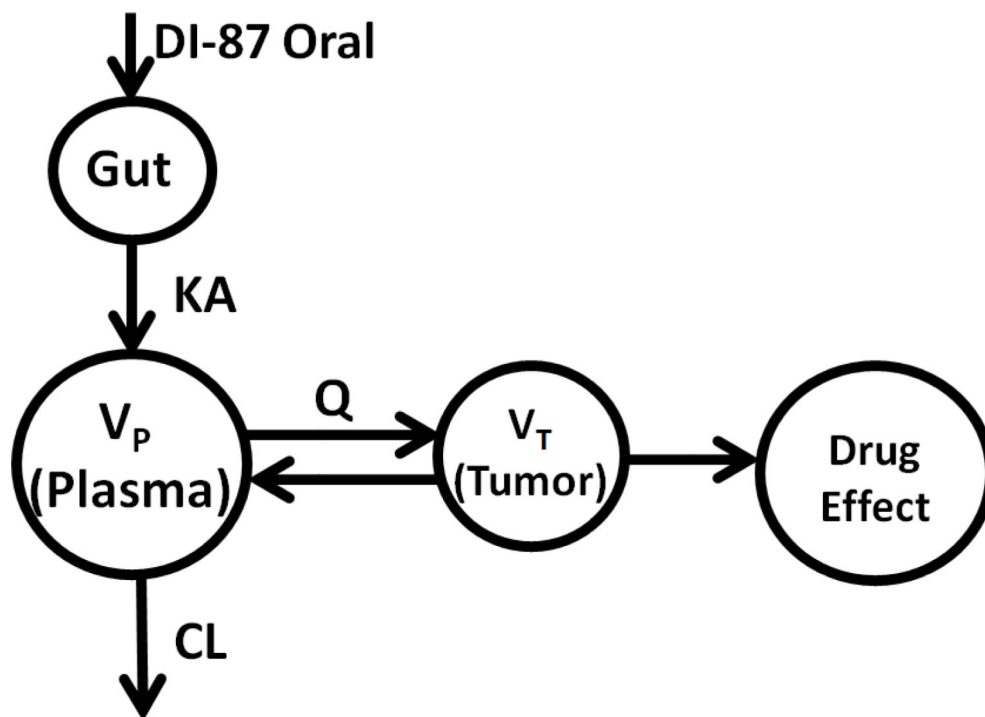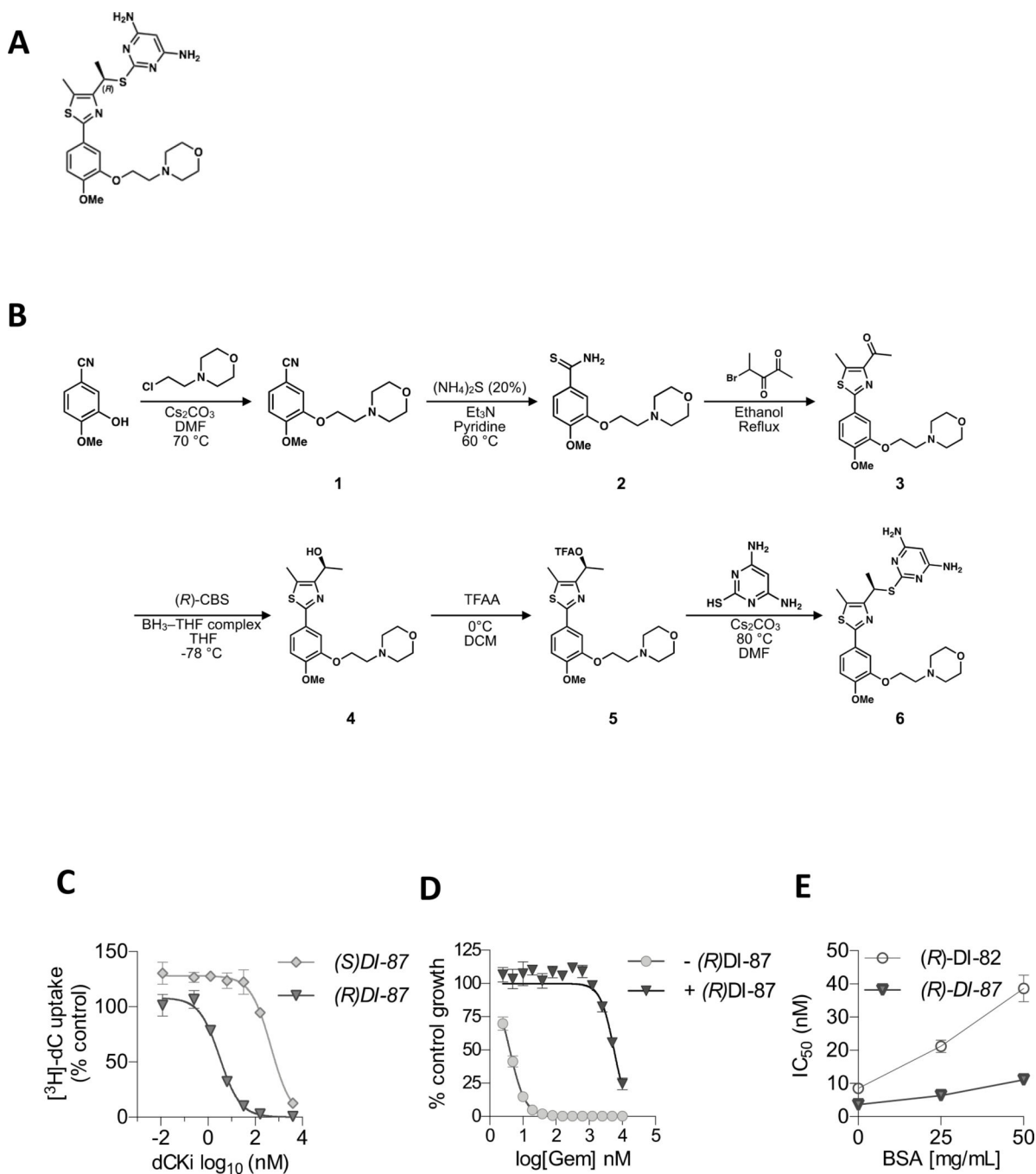
Figure 1:
Schematic of population PK-PD model. DI-87 is an oral drug which is absorbed from the gut with an absorption constant (KA). It distributes between the plasma volume (Vp) and tumor volume (Vt) with an intercompartmental clearance Q and is eventually cleared from the plasma compartment (CL). Tumor DI-87 concentrations lead to drug effect (dCK inhibition or growth inhibition). DCK inhibition with modeled with a sigmoid Emax indirect response model while growth inhibition was modeled with an Emax indirect response model.

A

B

C

D

E

Figure 2:
Synthesis and *in vitro* activity of DI-87. (A) Structure of DI87. (B) Synthetic route of DI-87. (C) IC$_{50}$ values determined using ^{3}H-dC uptake assay in CEM T-ALL cells to measure inhibition of dCK activity. (D) Dose response of DI-87 in CEM T-ALL cells treated with 10 nM Gemcitabine (n=4; mean±SD) for 72h determined using Cell Titer Glo. (E) Protein binding of DI-87 and *(R)*DI-82 assessed by comparing IC$_{50}$ of the compounds in presence of 25 and 50 mg/mL BSA (n=2; mean±SD).
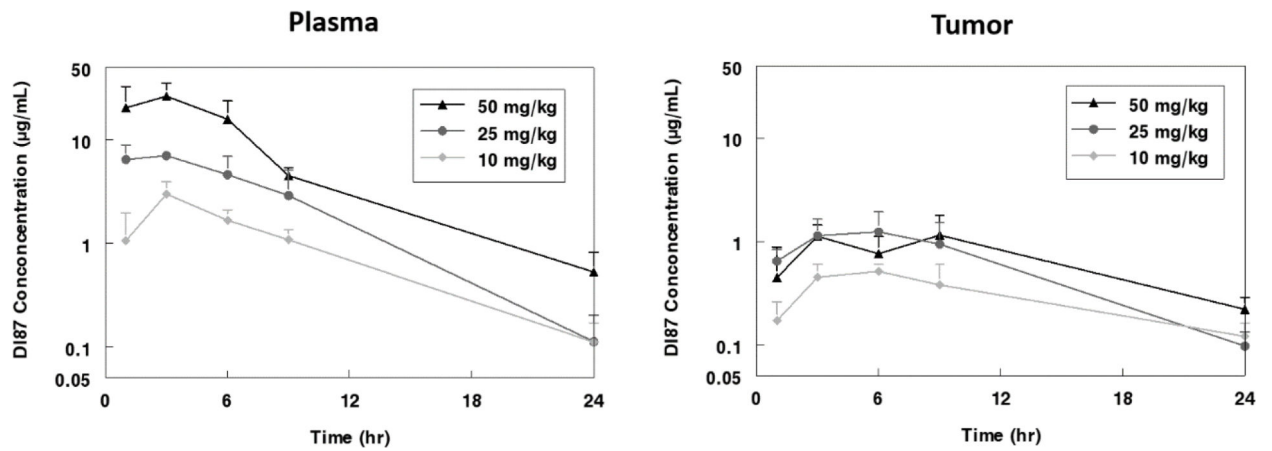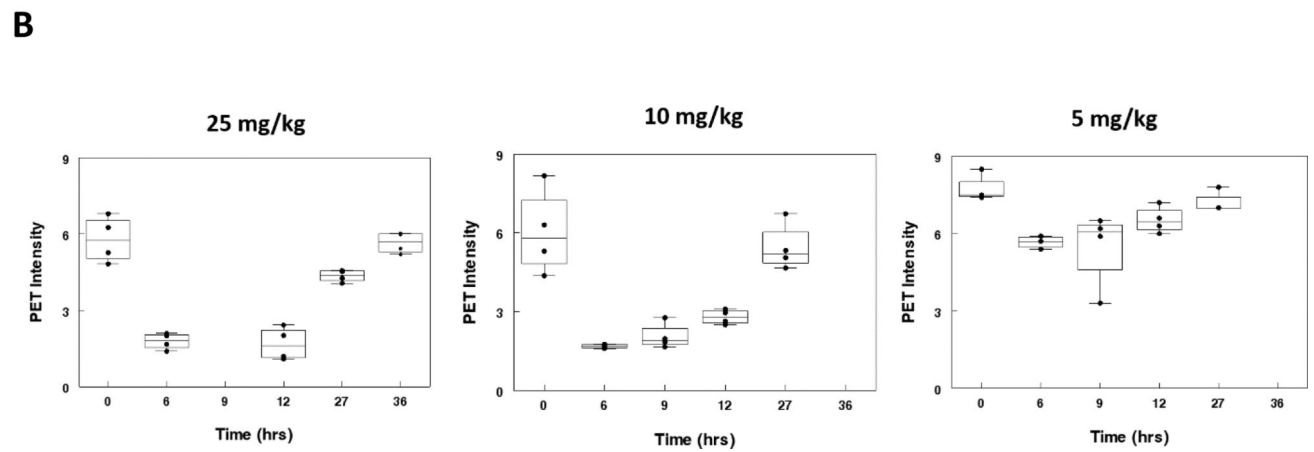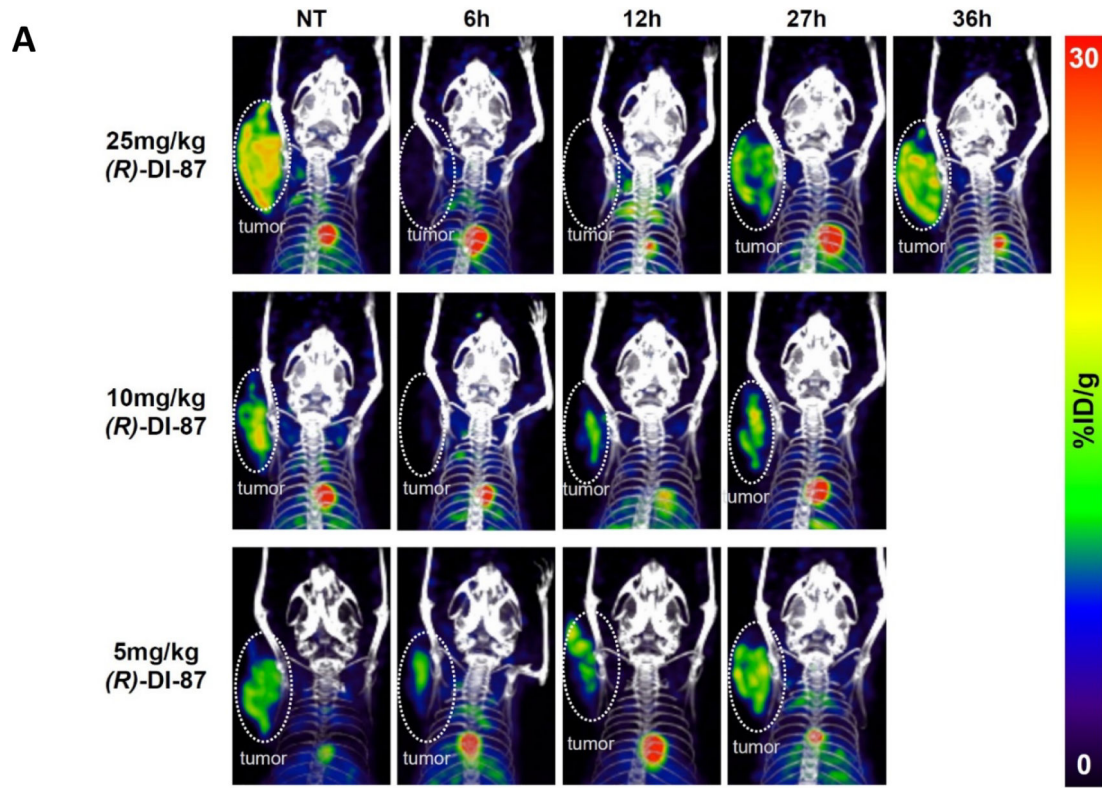
Figure 3:
Plasma and tumor concentrations. Each data point represents the plasma and tumor concentrations from a single mouse (n=5 per time point). Plasma concentrations are higher than tumor concentrations and have an earlier peak Tumor sizes varied between experiments thus it was difficult to determine if the tumor concentrations were linear.
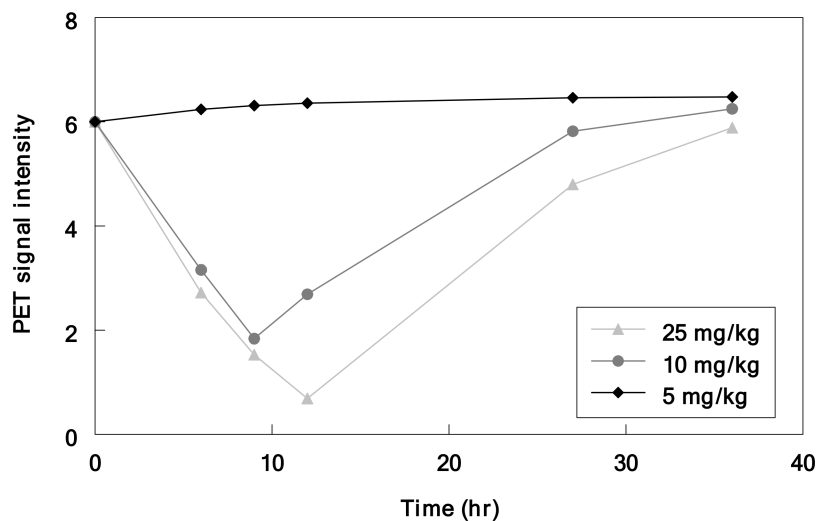
C

Figure 4:
dCK inhibition studies. A. dCK activity in tumors. DI-87 was administered as a single dose to mice and PET scans were completed following drug administration. dCK activity from representative mice over time is shown for 25 mg/kg, 10mg/kg, and 5 mg/kg. B. dCK activity as measured by PET scans. dCK inhibition was prolonged with higher doses of drug (25 mg/kg vs. 10 mg/kg). Minimal inhibition was seen at 5 mg/kg. C. Simulation of dCK activity for three doses of DI-87.
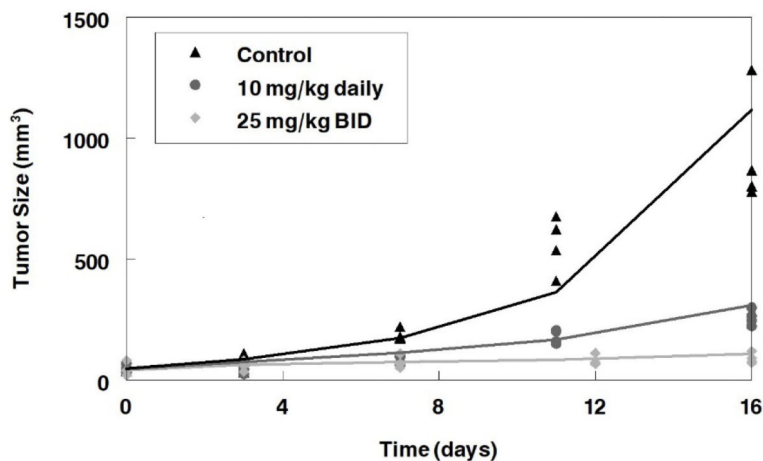
A
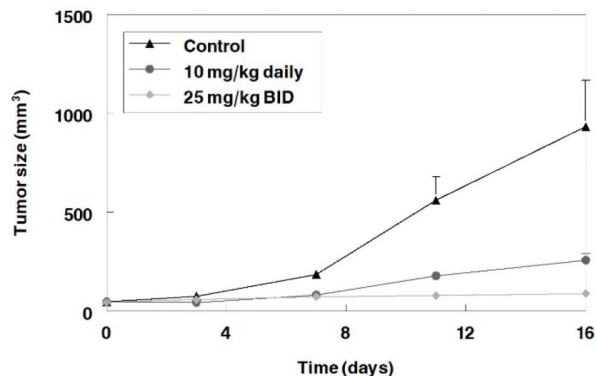
B

Figure 5:

A. Growth inhibition experiment. DI-87 was administered as multiple doses in combination with thymidine to mice. Near complete growth inhibition was seen with full DCK inhibition throughout the dosing interval (25 mg/kg BID). Data represent the mean and standard deviation of 5 mice. B. Growth inhibition model simulation. Solid lines represent simulations from final PK-PD model and symbols represent measured tumor size. Overall the model represents the data well.

Table 1:

PK-PD modeling parameter estimates

Plasma-Tumor PK model parameters		
	Parameter Estimate	**Standard Error**
CL (L/hr/kg)	0.46	0.03
V (L/kg)	2.78	0.22
KA (hr)	0.66 (FIXED)	.
Q (L/hr/kg)	0.0045	0.0013
Scalar	3.69	0.40
Half-life (hr) [*]	4.2	-
Eta1 (Scalar)	34.6%	0.08
Proportional Error	49.9%	0.04
DCK inhibition PK-PD model		
K_{out}	0.12	0.00011
E_{max}	1.20	0.00200
EC_{50}	0.31	0.00009
Gamma (Hill coefficient)	58.60	0.18500
K_{in}	0.76	0.00078
Additive Error	0.88	0.00025
Growth Inhibition PK-PD Model		
K_{out}	0.372	0.0973
E_{max}	1.06	0.2030
Growth Function Exp 1	0.00498	0.0011
Growth Function Exp 2	1.47	0.0399
EC_{50}	3.63	1.19
Intersubject Variability (E_{max})	14.1%	2.65%
Additive Error	0.20	0.02

[*] Half-life: 0.693/(CL/V)